scientific reports

OPEN

Interaction of various-sized particles in river flow

Niannian Fan[1,2 ✉], Qiang Zhong[3,4], Ruihua Nie[1] & Xingnian Liu[1]

Sediment transport is essential to the source-sink systems; however, the interaction between two complex multiscale nonlinear systems, turbulence of the river flow and wide size sediment, has heretofore restricted our understanding of sediment motion. We have conducted flume experiments deploying a video-based technique that records sediment transport rate of each particle size at 1 s resolution. The observations reveal detailed interactions between flow and particles of sizes ranging from 0.5 to 32 mm, such that small suspended particles (< ~ 5 mm) keep swirling in the wake vortices of the keystones (larger than 20 mm) until large to very-large-scale coherent structures destroy the wake vortices and bring the small particles downstream. Keystones destabilize consequently as the surrounding small and intermediate particles move, and in turn, a group of sheltered particles is entrained following the dislodging of the keystones. This heuristic model highlights the interactions of turbulence and different-sized particles.

In total, the rivers of the earth deliver more than 20 billion tons sediment to the oceans annually[1]. Sediment provides the major process linkage between hydrological factors[2], channel bed roughness[3], river channel morphology[4,5] and sedimentation archives[6]. All modern aspects of habitat restoration, infrastructure planning, and pollution remediation require knowledge or prediction of the response of sediment to flooding[7]. Current sediment transport models attempt to predict transport rates from average descriptors of flow and bed material, such as the time-averaged shear stress and bulk grain size distribution, without explicit scale correlations[8–12]. Problematically, sediment transport, especially for river beds composing of poorly sorted particles, is a stochastic process[13], and fluctuations of sediment transport rates orders larger than the mean have been shown in both field[14] and experimental observations[15]. Highlighting that at timescales approximating the duration of a single flood these models fail to capture integral aspects of the transport process, in particular local interactions between flow and bed roughness elements.

Consider a short section of nearly flat channel with a bed comprising poorly sorted natural sediment of mixed sizes exposed to a transporting flow (Fig. 1). At this scale, local interactions between near-bed turbulent structures and individual grains determine the entrainment behavior of particles[14,16–18]. This results in complex interactions between the flow and different-sized grains in transport, which may be described qualitatively using our conceptual model as Fig. 1. A large particle ($> D_{84}$), which requires energetic flow to mobilize it, generates a downstream wake. The large particle shelters smaller particles, which are often trapped in small-scale turbulent vortices behind the large grain (Fig. 1a), seldom leave the wake flow area until a large coherent turbulent structure comes (Fig. 1b). As the intermediate particles become entrained (Fig. 1c), the large particle becomes unstable and is dislodged. As a result, particles immediately upstream of the large particle are mobilized (Fig. 1d). In this conceptual model, the cascade of interactions between stream flow and mixed-size particles determine the sediment transport processes, and temporal variability in sediment transport rates for each size group. As a result, we expect differently sized particles to show distinct time-dependent patterns of transport.

To characterize the impact of the interactions between particles of various sizes in the proposed conceptual model, we conducted flume experiments with poorly sorted natural sediments (0.5–32 mm). The flume had a varying width (0.38–0.80 m) to force pool-riffle development[19], in order to more closely recreate natural river conditions. Moreover, our experiment is unique in that a time series of sediment transport rates were measured for individual size classes from a video based light table at a 1 s temporal resolution (see Figs. 2b, 3 and Supplementary Information Fig. 2). Details of the experimental conditions are available in Methods. We hope this study sheds light on the direction of mixed-size sediment transport and provides further impetus for both theoretical

[1]State Key Laboratory of Hydraulics and Mountain River Engineering, College of Water Resource & Hydropower, Sichuan University, Chengdu 610065, China. [2]Department of Geography, University of British Columbia, Vancouver V6T1Z2, Canada. [3]College of Water Resources and Civil Engineering, China Agricultural University, Beijing 100083, China. [4]Beijing Engineering Research Center of Safety and Energy Saving Technology for Water Supply Network System, China Agricultural University, Beijing 100083, China. ✉email: fanniannian@scu.edu.cn
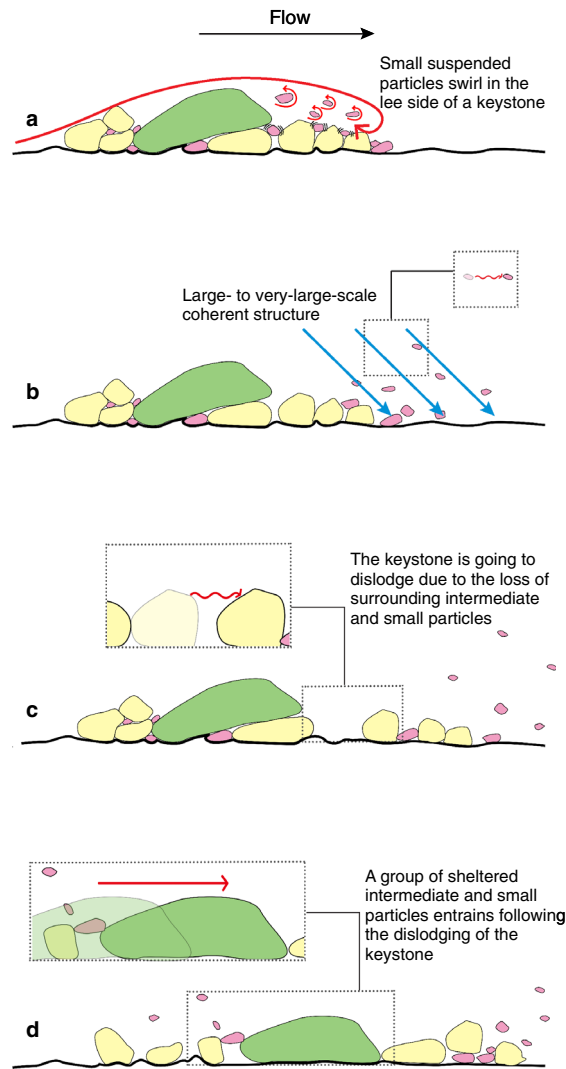
Figure 1. Sketch of flow and particle interactions in mixed size sediment transport. Flow is from left to right and the particles are grouped as small (pink), intermediate (yellow) and large (green) ones. (**a**) Small particles swirl in the lee of a large particle (key stone). (**b**) A group of small particles leaves the wake flow area in the lee of a key stone when a large to very-large-scale coherent flow structure passes by. (**c**) The intermediate particles are apt to be mobilized. (**d**) Intermediate and small particles supported by the keystone are mobilized after the keystone has become dislodged.

and experimental studies. The particle individual or collective motion of various sizes were studied. In addition, the interactions of various-sized particles and turbulence flow structures were also discussed.

Results

Various sized sediment transport rates.   Figure 3a displays the time series of bulk sediment transport rates at sampling intervals of 1 s, 8 s, 1 min and 6 min, respectively, along with the time-averaged mean. Figure 3b–f shows the sediment transport rates for each grain size subdivided into 0.5φ intervals (e.g., 1.4–2 mm, 2–2.8 mm, 2.8–4 mm, 4–5.6 mm…, 22.6–32 mm). The results show two distinct parts. First, as the sampling interval increases, the variability in sediment transport rate decreases. Second, larger particles show more intermittent transport characteristics, with the largest particles experiencing long periods of little motion followed by short lived periods of transport (see Fig. 3f).

As a stochastic time series, the variance of the sediment transport rates reflects the fluctuation magnitude, which decreases monotonically as the sampling interval increases. In our experiments, we expect that if each particle moves independently, a plot of variance and sampling interval in double-log space will have a slope of -1[8,15,20]. Over a sampling interval in which particles movements are correlated (e.g. due to collective entrainment), a slope closer to 0 appears[15]. As a result, for a variance-sampling interval plot in log–log space, a change in slope reflects a changing pattern of motion across timescales. In addition, those plots differ for each particle size group, thus a cascade of interactions between each particle size group can be revealed. Moreover, if the
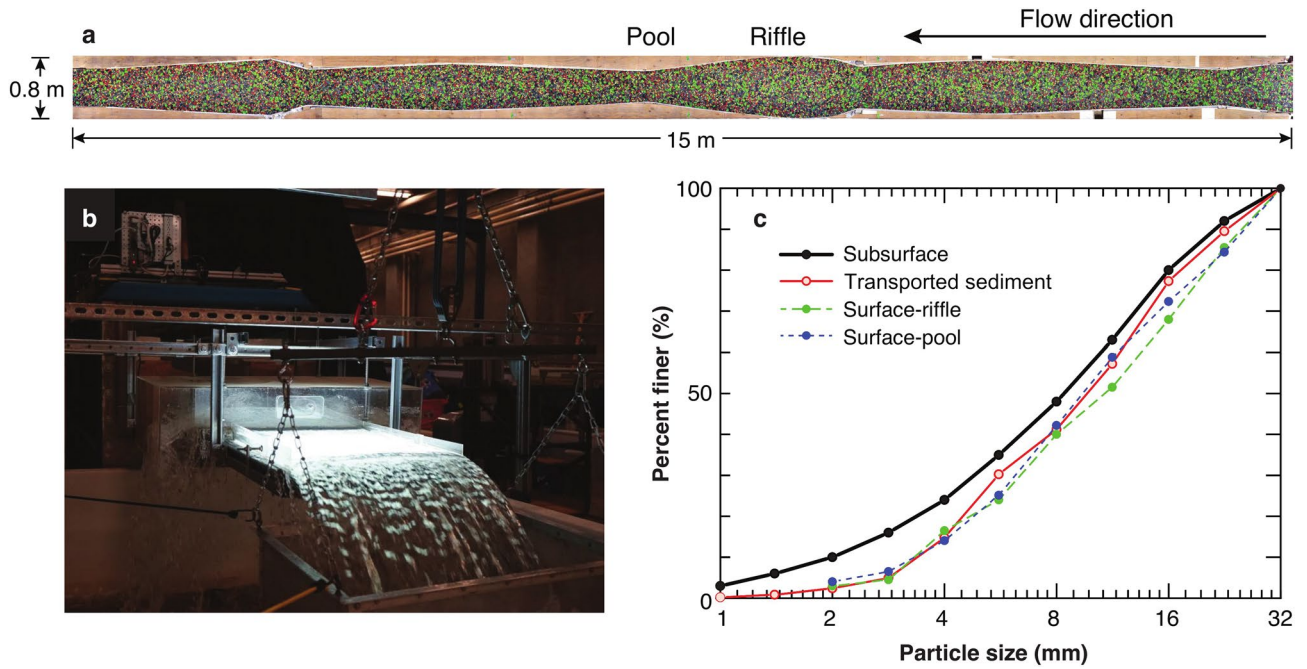
Figure 2. Overview of the experiment. (**a**) Image of the flume. The length of the flume was 18 m in total, but we had stitched photographs of only the middle 15 m. (**b**) Light table and basket at the outlet of the flume. (**c**) Size distribution for subsurface and feeding sediment (solid black line), transported sediment (solid red line), surface in riffle (dashed green line) and pool (dashed blue line) at the end of experiment.
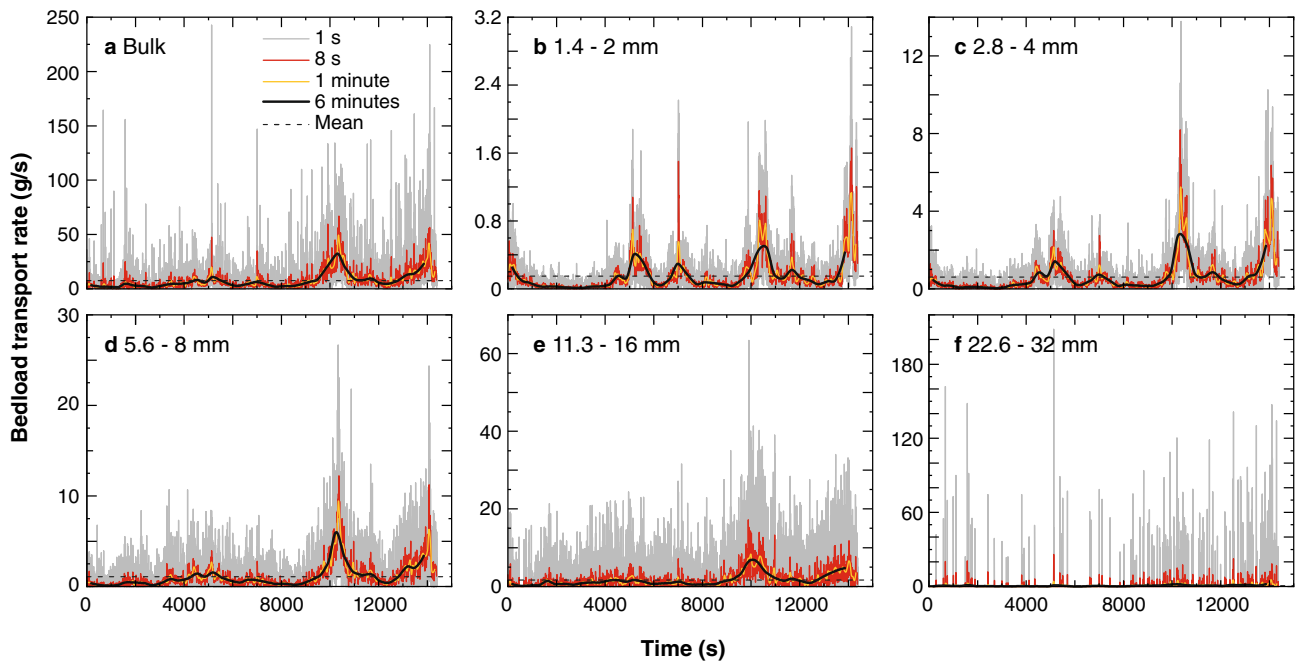
Figure 3. Time series of sediment transport rates collected for 4 h at sampling interval of 1 s, 8 s, 1 min and 6 min shown in grey, red, yellow and black solid lines respectively. The mean value is indicated as a black dashed line, note that *y*-axis scale varies for each plot. Subplot (**a**) is for the bulk sediment, and Subplots (**b**, **c**, **d**, **e** and **f**) are for particle size groups of 1.4–2 mm, 2.8–4 mm, 5.6–8 mm, 11.3–16 mm and 22.6–32 mm, respectively. Note that the longer the sampling interval, the smoother the sediment transport rates show.

timescales of a turbulence structure coincides with an observed time scale of particle motion it suggests this turbulence structure drives that pattern of particle motion.

Figure 4a–f displays the relation between variance (scaled by the power of the mean value of sediment transport rate) and the sampling interval for the bulk and grain-size specific sediment transport rates. In Fig. 4a, the bulk transport rates can be divided into three distinct sampling interval ranges using the slope of the variance. At
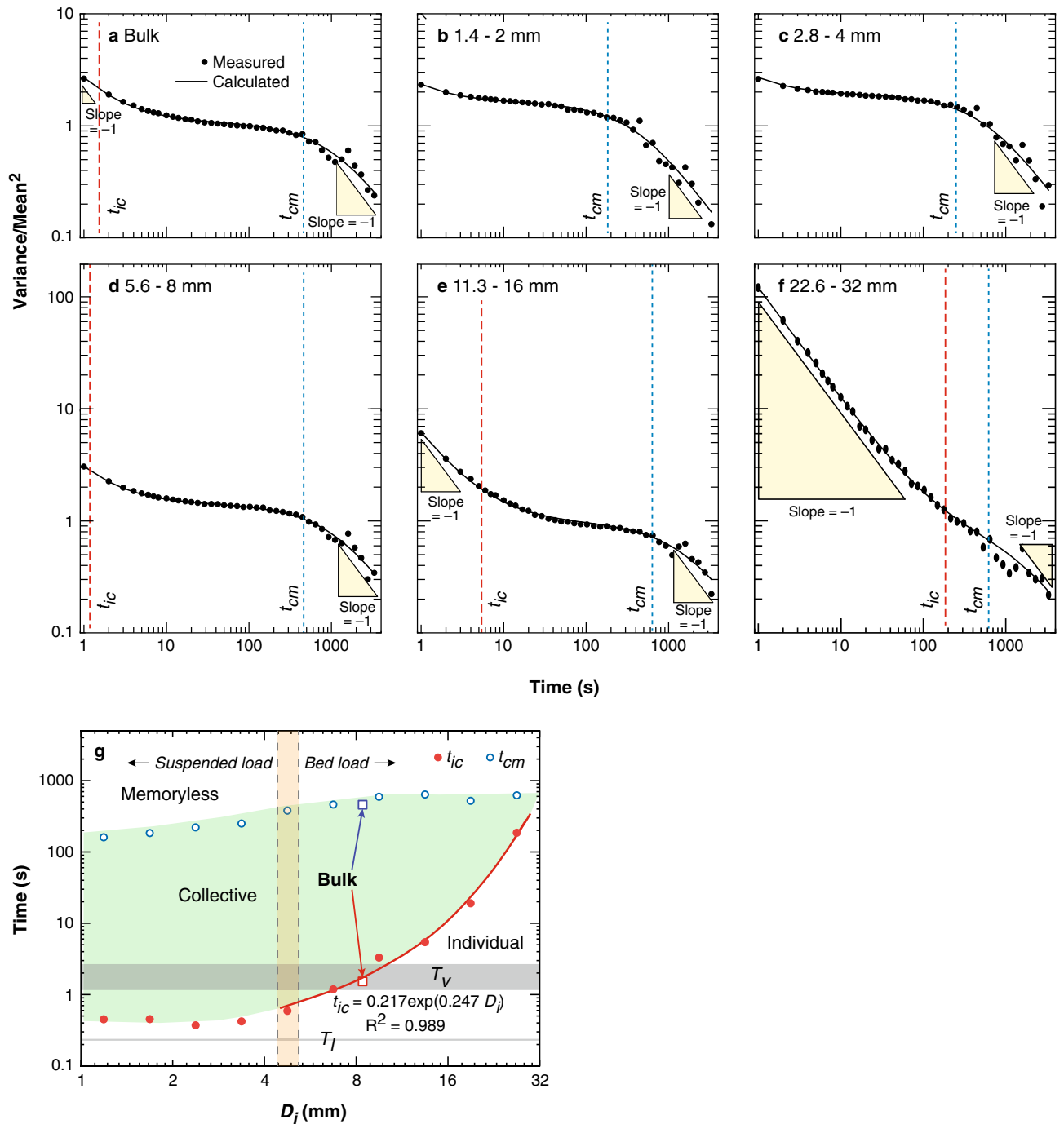
Figure 4. Normalized variance of sediment transport rates at different time scales. Subplot (**a**) is for the bulk sediment and Subplots (**b**–**f**) are for particle size groups of 1.4–2 mm, 2.8–4 mm, 5.6–8 mm, 11.3–16 mm and 22.6–32 mm, respectively. Two critical times, t_{ic} (red dashed line) and t_{cm} (blue dashed line) define the three regimes for variance decays at a slope of −1, 0 and −1 respectively. (**g**) Relations between critical times (t_{ic}, red dots and t_{cm}, blue dots) and particle sizes summarized from subplot (**a**–**f**), time scales of turbulence structures also show.

small sampling intervals, the variance decays approach a slope of −1, suggesting that particle motions are individual and independent without correlation, which we define as individual time scale. In intermediate sampling intervals (2–400 s), however, the variance remains almost constant, particle motion is dominated by collective entrainment events, resulting in highly correlated sediment transport rates which we define as the collective timescale. At longer timescales, so many collective entrainment events occur that the memory between each event vanishes, we term this as the memoryless timescale. The time scale-variance relation could be fit using Eq. (1) (see "Methods" Section for details). Demarcating these timescales are two critical times, t_{ic} (separating

individual and collective time scales) and t_{cm} (separating collective and memoryless time scales) (See Eq. 1 in "Methods" Section), marked as the red and blue dashed lines respectively.

Interactions of turbulence and particles. Figure 4b–f allow for the comparison of these timescales across grain size classes, note that the 1 s sample time normalized variance for keystone (Fig. 4f) is at least one order larger than other particles (Fig. 4b–e). Figure 4g displays the relationship between particle size and the critical times (t_{ic} and t_{cm}). It needs to note that, D_{50} plotted with both t_{ic} and t_{cm} for the bulk sediment fits the general trend of individual sediment size classes, which might support the convention that although the detailed transport processes for poorly sorted particles are more complex than for uniform particles[21–23], D_{50} could serve as a proxy for the size of bulk sediment[24].

Discussion

As Fig. 4g, the relationship of t_{ic} and particle size shows two distinct segments with critical size of ~5 mm, corresponding to be the critical size boundary (4.4–5.4 mm) for suspended load and bed load (see "Methods" Section). t_{ic} keeps almost constant values (~0.4 s) for suspended load, which is in the range between T_l ~ 0.25 s and T_v ~ 2 s (Fig. 4g), supporting that large- to very-large-scale coherent flow structures (LSMs to VLSMs, in the order of 1 to 10 times the flow depth[25]) displace the suspended particles in the lee of keystones collectively[14]. Meanwhile, the relative weak wake vortices of the keystones, if drive downstream motion of suspended particles, only occasionally move them downstream individually, contributing individual motion scale smaller than t_{ic} (see "Methods" Section).

Figure 4g also shows the weak relationship between t_{cm} (separating collective and memoryless time scales) and particle size, which is interpreted to result from that following the dislodging of a keystone, a group of particles ranging over a wide size range sheltered by the keystone entrained simultaneously and collectively. However, keystones, the largest particles on the bed, are not sheltered by any larger particles, therefore t_{ic} and t_{cm} emerges, such that keystones do not experience collective entrainment.

The increasing of t_{ic} with the particle size for bed load illustrates the complex flow-particle and various-sized particle interactions. Firstly, the probability of occurrence of higher impulse events that can move larger particles decreases rapidly with the increasing of the particle size[21]. Secondly, particles interact with each other by granular contact network supported force chains[26,27]; with larger particles having more effective force chains[28]. The combination of these two factors may lead to the exponential growth of t_{ic}.

It is important to address that the turbulence structure and mix-sized grain interactions we studied here is in a much smaller time scale than morphology adjustment or motion of bed forms[22]. For example, the periodic filling and eroding of pool-riffle morphology is in the scale of ~20 h (Supplementary Information Fig. 1), two or three orders longer than t_{cm} (order of 100 s). Nevertheless, the ways that particles interact at smaller spatial and temporal scales to drive riverbed morphology adjustments at larger scales warrants further study.

The results observed in this experiment are similar to the conceptual model elucidated in Fig. 1. Although our heuristic model is likely invalid during strong flow conditions capable of mobilizing all particle sizes, it is applicable for sediment transport in most gravel-bed alluvial rivers as shear stress during floods is usually only slightly larger than the critical shear stress for entrainment[29]. Exceptions to this generalization include outburst floods from dam breaks[30] or very high sediment supplied conditions[31], for those two conditions, we expect that particles move collectively and individual-grain transport does not exist.

Conclusion

In this study, we observed poorly sorted sediment transport from flume experiments for steady transport condition. Size-specific transport rates at a temporal resolution of 1 s were obtained, allowing us to reveal grain/grain interactions and where possible, to reveal grain/turbulence flow interactions.

From the variation of the time series of size-specific sediment transport rates, we revealed both individual and collective motions at certain time scales. For smaller, suspendable sizes, the time scale boundary between individual and collective (t_{ic}) corresponds to the time scale of large to very large turbulent fluctuations. For larger sizes in the mixture, t_{ic} increases with grain size. The upper limit of the collective transport time scale (t_{cm}) is defined by the upper limit for individual transport of the coarsest grain size, suggesting that the time scale for the occasional entrainment of these keystone clasts defines the longest time variation of the bed, transport at longer time scales is uncorrelated and independent (memoryless) of shorter time scales. This time scale (roughly 500 s in our experiment) can be used to define the smallest time scale appropriate for modeling using transport formulas based on mean flow and bed properties.

We acknowledge that the time scales for turbulence flow structure were calculated from the flow condition, instead of direct measurement. Detailed in situ observations of turbulence and grain motion at various flow and sediment conditions (e.g., armoring and aggrading), or considering the sediment shape[32] are required in future studies.

Methods

Experimental procedure. The flume[19,33] is 18 m long with the bed inclined at a 1.5% slope. The width is variable, ranging from 0.38 to 0.80 m (Fig. 2a), allowing for morphodynamic development in different flume sections. The particle size distribution of the initial bed and the feeding sediment was the same, which was poorly sorted natural sand and gravel with sizes ranging from 0.5 to 32 mm, with a D_{50} of 8.4 mm. The sediment was sieved at 0.5φ intervals (e.g., 1.4–2 mm, 2–2.8 mm, 2.8–4 mm, 4–5.6 mm…, 22.6–32 mm), and different size classes were painted with different colors. Water was recirculated and discharge was controlled by a variable

frequency pump, while sediment was fed to the flume inlet by a conveyor belt and collected with a basket trap at the flume outlet. See Table 1 for the brief information of the flume experiment.

Flow discharge was kept constant at 50 Liters/s. Riffles (in the wide sections) and pools (in the narrow sections) were formed from an initially levelled bed, after running the flume for 81 h without sediment feed until sediment load transport rate was very low (0.079 g/s). After these low transport rates were achieved (indicating a stable bed), sediment with a rate of 10.9 g/s (dashed line in Supplementary Information Fig. 1) was fed at the flume inlet and these conditions were run for 68.5 h (Supplementary Information Fig. 1). At approximately 36 h, the sediment transport rate became equivalent to the feeding rate indicating that quasi steady-state conditions had been reached. Detailed sediment transport rates were obtained from a video-based light table[34] (see Supplementary Information Fig. 2, the interval of 42.5–46.5 h marked grey in Supplementary Information Fig. 1), at time scales of 1 s for different sizes at 0.5φ interval. Although the cutoff value of the smallest particle sizes was 0.5 mm, transport rate data from the light table were not reliable for particles < 1 mm[20] so they were not used for further analysis.

From 42.5 to 46.5 h, the total sediment mass from the video-based method was calculated as 109.4 kg, while 110.7 kg of sediment was collected from the basket at the outlet of the flume, indicating a very small (1.2%) under-estimation bias. Also, the particle size distributions derived from the video-based method and sieving from basket collected sediment are very close (Supplementary Information Fig. 3), indicating that the video-based method performed well.

Model for fitting the three ranges of variance–time relations.
Rearranging from the model shown in reference[15], Eq. (1), the function between time scale and (normalized) variance of sediment transport rate, was obtained as:

$$\text{Var/Mean}^2(\Delta t) = \frac{a}{\Delta t}\left\{\frac{2t_{\text{cm}}}{t_{\text{ic}}}\left[1 - \frac{t_{\text{cm}}}{\Delta t}\left(1 - e^{-\frac{\Delta t}{t_{\text{cm}}}}\right)\right] + 1\right\} \tag{1}$$

where the variance (Var) was normalized by the square of the mean (Mean) value, t_{ic} and t_{cm} are the critical times dividing individual, collective and memoryless time scales, respectively. a is a constant coefficient for calibration.

We acknowledge that for particles smaller than 5.6 mm, the t_{ic} are smaller than the resolution of sediment transport rate time series in our experiment (1 s) as shown in Fig. 4b–c, and thus the values of t_{ic} are obtained by extension of the model as Eq. (1). However, the trends for − 1 slope when time scales approach to 1 s are obvious as Fig. 4b and c, as a result, we consider the calibrated values of t_{ic} from Eq. (1) are reliable.

Estimation of flow structure time scales.
The period of the very-large-scale coherent structures, Tv, is calculated as reference[35]

$$T_v = 5.7B^{0.6}h^{0.4}/\text{u} \tag{2}$$

where B, h and u are the channel width, depth and average cross-section velocity, respectively. In pool and riffle sections, the values of B are 0.38 and 0.80 m and the value of h are 13.5 and 8.4 cm, the values of u are calculated to be 0.97 and 0.76 m/s, respectively from the constant discharge Q = 50 L/s. As a result, T_v is calculated to be in the range of 1.5–2.4 s.

The period of the large-scale coherent structure is calculated as reference[17]

$$T_l = 2\text{h}/\text{u} \tag{3}$$

and T_l is calculated to be in the range of 0.22–0.27 s.

The period of wake vortices shedding of the keystones is calculated as[36,37]

$$T_w = D_k/(S_t u) \tag{4}$$

where D_k is the dimension of keystones (~ 25 mm), S_t is the Strouhal number, and here $S_t = 0.19$ as the keystone Reynolds number Re_d is in the range of $1.8–2.5 \times 10^4$. As a result, T_w is calculated to be in the range of 0.11–0.14 s.

Estimation of size boundary for bed load and suspended load.
The threshold for sediment suspension was calculated based on the ratio of shear velocity u_* and particle terminal settling velocity w_s as $u_*/w_s = 0.4$, particles were suspended load or bed load if $u_*/w_s > 0.4$ or < 0.4, respectively[38], given $u_* = 11.5$–12.9 cm/s in our experiment, we calculated the particles in the threshold for suspension had w_s in the range of 28.8–32.2 cm/s. w_s was the function of particle size D as reference[39]

Width (cm)	Depth (cm)	Slope	Flow rate (L/s)	Reynold number (10⁴)	Froude number	Sediment size (mm)	Sediment feed rate (g/s)
38–80	3.4–11	1.5%	50	6.26–13.2	1.56–3.19	0.5–32	10.9

Table 1. Brief information of the flume experiment.

$$w_s = \frac{RgD^2}{C_1 v + \sqrt{0.75 C_2 RgD^3}} \qquad (5)$$

where R is submerged specific gravity (1.65 for the particles in our experiment), g is gravitational acceleration, which equals to 9.81 m/s², $C_1 = 20$ and $C_2 = 1.1$ are constants for natural particles, and v is the kinematic viscosity of water, which equals to 10^{-6} m²/s.

Then critical size for particle suspension in our experiment was calculated to be in the range of 4.4–5.4 mm.

Data availability
All data are available in the main text and the Supplementary Material.

References

1. Syvitski, J. P. M., Vorosmarty, J. C., Kettner, J. A. & Green, P. Impact of humans on the flux of terrestrial sediment to the global coastal ocean. *Science* **308**, 376–380 (2005).
2. Church, M. Bed material transport and the morphology of alluvial river channels. *Annu. Rev. Earth Planet. Sci.* **14**, 325–354 (2006).
3. Gomez, B. Bedload transport. *Earth Sci. Rev.* **31**(2), 89–132 (1991).
4. Turowski, M. J., Badoux, A., Leuzinger, J. & Hegglin, R. Large floods, alluvial overprint, and bedrock erosion. *Earth. Surf. Proc. Land.* **38**, 947–958 (2013).
5. Gasparini, M. N., Tucker, E. G. & Bras, L. R. Downstream fining through selective particle sorting in an equilibrium drainage network. *Geology* **27**, 1079–1082 (1999).
6. Lee, A., Enters, D., Huang, J. S., Liou, S. Y. H. & Zolitschka, B. An automatic sediment-facies classification approach using machine learning and feature engineering. *Commun. Earth Environ.* **3**, 294 (2022).
7. Hassan, A. M. *et al.* Salmon-driven bed load transport and bed morphology in mountain streams. *Geophys. Res. Lett.* **35**, L04405 (2008).
8. Einstein, A. H. Der Geschiebetrieb als Wahrscheinlichkeits problem. Swiss Federal Institute of Technology Zurich (1937).
9. Meyer-Peter, E. & Müller, R. Formulas for bed load transport. In *International Association of Hydraulic Research, 2nd Meeting Documents*. (IAHR, Stockholm, 1948).
10. Liu, X. & Chen, Y. Transport of nonuniform bed load. *J. Chengdu. Univ. Sci. Tech.* **34**, 29–36 (1987) (**in Chinese with English abstract**).
11. Parker, G. Surface-based bedload transport relation for gravel rivers. *J. Hydraul. Res.* **28**, 417–436 (1990).
12. Venditti, G. J. *et al.* Mobilization of coarse surface layers in gravel-bedded rivers by finer gravel bed load. *Water Resour. Res.* **46**, W07506 (2010).
13. Gomez, B. & Church, M. An assessment of bed load transport formulae for gravel-bed rivers. *Water Resour. Res.* **25**, 1161–1186 (1989).
14. Drake, G. T., Shreve, L. R., Dietrich, E. W., Whiting, J. P. & Leopold, B. L. Bedload transport of fine gravel observed by motion-picture photography. *J. Fluid Mech.* **192**, 193–217 (1988).
15. Ma, H. B. *et al.* Bed load transport over a broad range of timescales: Determination of three regimes of fluctuations. *J. Geophys. Res. Earth.* **119**, 2653–2673 (2014).
16. Nelson, M. J., Shreve, L. R., Mclean, R. S. & Drake, G. T. Role of near-bed turbulence structure in bed-load transport and bed form mechanics. *Water Resour. Res.* **31**, 2071–2086 (1995).
17. Roy, G. A., Buffin-Blanger, T., Lamarre, H. & Kirkbride, D. A. Size, shape and dynamics of large-scale turbulent flow structures in a gravel-bed river. *J. Fluid Mech.* **500**, 1–27 (2004).
18. Hardy, J. R., Best, L. J., Parsons, R. D. & Marjoribanks, I. T. On the evolution and form of coherent flow structures over a gravel bed: Insights from whole flow field visualization and measurement. *J. Geophys. Res. Earth.* **121**, 1472–1493 (2016).
19. Hassan, M. A. *et al.* Experiments on the sediment transport along pool-riffle unit. *Water Resour. Res.* **58**, e2022WR0327969 (2022).
20. Elgueta-Astaburuaga, A. M., Hassan, A. M., Saletti, M. & Clarke, G. K. C. The effect of episodic sediment supply on bedload variability and sediment mobility. *Water Resour. Res.* **54**, 6319–6335 (2018).
21. Diplas, P., Dancey, L. C., Celik, O. A., Valyrakis, M. & Akar, T. The role of impulse on the initiation of particle movement under turbulent flow conditions. *Science* **322**, 717–720 (2008).
22. Dhont, B. & Ancey, C. Are bedload transport pulses in gravel bed rivers created by bar migration or sediment waves?. *Geophys. Res. Lett.* **45**, 5501–5508 (2018).
23. Lee, B. D. & Jerolmack, D. Determining the scales of collective entrainment in collision-driven bed load. *Earth Surf. Dyn.* **6**, 1089–1099 (2018).
24. Wilcock, R. P. & Crowe, C. J. Surface-based transport model for mixed-size sediment. *J. Hydraul. Eng.* **129**, 120–128 (2003).
25. Zhong, Q., Li, D., Chen, Q. & Wang, X. Coherent structures and their interactions in smooth open channel flows. *Environ. Fluid Mech.* **15**, 653–672 (2015).
26. Ferdowsi, B., Ortiz, P. C., Houssais, M. & Jerolmack, J. D. River-bed armouring as a granular segregation phenomenon. *Nat. Commun.* **8**, 1–10 (2017).
27. Frey, P. & Church, M. How river beds move. *Science* **325**, 1509–1510 (2009).
28. Zhang, C., Xu, M., Hassan, A. M., Chartrand, M. S. & Wang, Z. Experimental study on the stability and failure of individual step-pool. *Geomorphology* **311**, 51–62 (2018).
29. Phillips, B. C. & Jerolmack, J. D. Self-organization of river channels as a critical filter on climate signals. *Science* **352**, 694–697 (2016).
30. Cook, L. K., Andermann, C., Gimbert, F., Adhikari, R. B. & Hovius, N. Glacial lake outburst floods as drivers of fluvial erosion in the Himalaya. *Science* **362**, 53–57 (2018).
31. Pfeiffer, M. A., Finnegan, J. N. & Willenbring, K. J. Sediment supply controls equilibrium channel geometry in gravel rivers. *P. Natl. Acad. Sci. U. S. A.* **114**, 3346–3351 (2017).
32. Deal, E. *et al.* Grain shape effects in bed load sediment transport. *Nature* **613**, 298–302 (2023).
33. Chartrand, M. S., Jellinek, M. A., Hassan, A. M. & Carles, B. F. Morphodynamics of a width-variable gravel bed stream: New insights on pool-riffle formation from physical experiments. *J. Geophys. Res. Earth* **123**, 2735–2766 (2018).
34. Zimmermann, E. A., Church, M. & Hassan, A. M. Video-based gravel transport measurements with a flume mounted light table. *Earth Surf. Proc. Land.* **33**, 2285–2296 (2008).
35. Cameron, M. S., Nikora, I. V. & Stewart, T. M. Very-large-scale motions in rough-bed open-channel flow. *J. Fluid Mech.* **814**, 416–429 (2017).

36. Liu, C. & Nepf, H. Sediment deposition within and around a finite patch of model vegetation over a range of channel velocity. *Water Resour. Res.* **52**, 600–612 (2016).
37. Norberg, C. An experimental investigation of the flow around a circular cylinder: Influence of aspect ratio. *J. Fluid Mech.* **258**, 287–316 (1994).
38. Niño, Y., Lopez, F. & Garcia, M. Threshold for particle entrainment into suspension. *Sedimentology* **50**, 247–263 (2003).
39. Ferguson, R. & Church, M. A simple universal equation for grain settling velocity. *J. Sediment. Res.* **74**, 933–937 (2004).

Acknowledgements

Author contributions

N.F. conducted the experiments. Q.Z. developed the turbulent flow analysis. N.F. and Q.Z. drafted the paper, which was then reviewed by all of the co-authors.

Competing interests

The authors declare no competing interests.

Additional information

Supplementary Information The online version contains supplementary material available at https://doi.org/10.1038/s41598-023-37460-y.

Correspondence and requests for materials should be addressed to N.F.

Reprints and permissions information is available at www.nature.com/reprints.

Publisher's note Springer Nature remains neutral with regard to jurisdictional claims in published maps and institutional affiliations.